Experimental and Numerical Investigation of Local Scouring around Bridge Piers in Different Geometric Shapes at a 90° Convergent meander

Mousa Rasaei [1]
Sohrab Nazari [2]

Abstract

The presence of several convergent meanders is a basic characteristic of natural flowing rivers. It is important to construct bridge piers in different geometric shapes at convergent meanders. The formation of secondary flows at meanders and their enhancement by the convergence effect can bring complexities and irregularity in the erosion pattern around bridge piers. The present study experimentally and numerically investigates the effects of the geometric shapes of bridge piers on local scour around piers at a 90° convergent meander. Tests were carried out within a channel with a 90° convergent meander and a centerline radius of 170 cm. Cylindrical piers with the diameters of 40 and 60 mm and cubic piers with the sizes of 40×40 and 60×60 mm were placed at the center of the meander, investigating scour in clear-water conditions. Also, a three-dimensional SSIIM-2 model was employed to simulate the problem and compare the results to the experimental ones. The results indicated that the shapes and sizes of the piers affected the scour depth, and the maximum scour depth was estimated to be smaller around the cylindrical piers than around the cubic piers in all the tests. Moreover, convergence-induced contraction along with the placement of the piers at the meander enhanced scour around the piers. The numerical SSIIM-2 results were found to be in a good agreement with the experimental results.

[1] Department of Civil Engineering, Dehdasht Branch, Islamic Azad University, Dehdasht, Iran, rasaei.iau@gmail.com (**Corresponding author**)
[2] Department of Civil Engineering, Eqlid Branch, Islamic Azad University, Eqlid, Iran.

1. Introduction

The presence of several meanders in flow paths is a basic characteristic of natural rivers. As they have a specific flow pattern known as the helical flow, meanders have been considered by hydraulic engineers. The helical flow at a meander induces erosion at the outer curve of the meander and sediment at the inner curve. Sedimentation and erosion do not typically occur uniformly at a meander and sometimes reduce the meander width along the path, making it convergent, as shown in Figure 1. On the other hand, the placement of the bridge piers with different geometric shapes at the convergent meander is one of the important issues. The formation of secondary flows and their enhancement by the convergence effect can bring complexities and irregularity in the erosion pattern around bridge piers.

Figure 1.View of a natural river with a 90° convergent meander [1]

Flow hydraulics and scour around bridge piers have been experimentally and numerically studied by different researchers, some of which are mentioned in the following:

Tison [2] experimentally studied local scour around rectangular, triangular, aerodynamic, and lenticular bridge piers. Yen [3] performed experiments in a channel bend to study the equilibrium bed configuration and flow characteristics. Georgiadou and Smith [4] conducted one of the earliest studies on flow hydraulics and sedimentation in channels with convergent meanders. They incorporated a 90° convergent meander with a centreline radius of 150 cm. The channel began with a width of 90 cm upstream and reached a width of 45 cm downstream. The results indicated the maximum velocity path to be near the inner curve of the convergent meander. Melville and Chiew [5] investigated the time development of the scour depth around cylindrical bridge piers in clear-water conditions. They demonstrated that the scour depth occurred to be 50-80% of the equilibrium scour depth, depending on the flow velocity, after a time as long as 10% of the equilibrium time. Olsen [6] modelled and analyzed the secondary flows and sediment transfer of a narrow channel with a 90° meander. Abouzeid et al. [7] investigated the flow and local scour variation around single pier and the interaction effect between bridge piers using 3D flow model. It was noticed that the maximum scour depth for

circular pier is less than that for rectangular one for both single and double pier cases. Dey and Raikar [8] evaluated horseshoe vortex development in scour holes around cylindrical and cubic bridge piers. Larger scour parameters were obtained for the cubic piers than for the cylindrical piers in all the flow conditions. Sanoussi and Habib [9] studied the effects of sloped and rounded bridge pier noses on local scour. They concluded that the sloped pier noses led to smaller scour depths. Sanei et al. [10] suggested that a 90% rise in the pier diameter raised the scour depth by 180%. Experimental investigation of Scouring and flow field around a spur dike in a 90° bend were conducted by Fazli et al. [11]. Their investigation results indicated, the maximum depth of scour is correlated to the Froude numbers, lengths and the locations of spur dike. Masjedi et al. [12] carried out tests in a Plexiglas laboratory flume with a 180° meander, a centreline radius of 2.8 m, a radius of 0.6 m, and an R/B ratio of 4.67 in order to explore the effects of the geometric shape of piers on the control of scour around the piers at river meanders. They investigated scour around piers in clear-water conditions by placing a cylindrical pier with a diameter of 6 cm and a cubic pier with a semi-circular nose, a width of 6 cm, and a length of 18 m within the flume at the angles of 0, 30, 60, and 90 degrees, the flow rates of 24, 28, 30, 32 l/s, and a fixed scour depth of 12 cm around the piers in clear-water conditions. Natural sand with a grading degree of D_{50}=2 mm and a uniformity coefficient of 1.3 was applied to the bottom of the flume. The results indicated that the maximum scour depth alternated for the cylindrical pier and the cubic one with a semi-circular nose, occurring in the first half of the meander at an angle of 60 degrees. Also, the scour of the cylindrical pier was smaller than that of the cubic pier with a semi-circular nose. A rise in the flow rate raised the scour depth in all the conditions. Ghobadian et al. [13] used numerical model to study three-dimensional flow patterns in a 180° bend, one with a uniform (0.6 m) width and other with a divergent (0.6 m to 0.75 m) width. They in this research, investigated and compared the Flow characteristics such as stream wise and vertical velocity profiles, primary and secondary flows, stream wise and span wise slopes of water surface, bed shear stress distribution and helical flow strengths. Results indicated that in a divergent bend, the path of maximum velocities at plane near water surface crosses the channel's centre line at about 50°, while in uniform bend this occurs at about 55°. However, the path of maximum velocity tangent to outer wall of uniform bend at about 90°-100°, while in divergent bend occurred at about 80°. On the other hand, Verification using experimental data showed that the SSIIM numerical model can successfully simulate flow fields in bends. Sabita and Maiti [14] studied local scour around a circular pier within an open channel. Their results indicated that the scour depth increased as the time and flow rate increased; however, the scour depth changed nonlinearly. Zulhilmi et al. [15] analyzed scour depths and patterns around a single and a double pier placed in a straight channel. Fael et al. [16] examined the effect of the shape and angle of the pier on a single pier scour depth under clear water flow. They considered five different pier shapes, such as circular, rectangular, square and round nosed, oblong and zero-spacing pile groups, and made a comparative study with different dimensions of shape. The result of this study also showed that the value of the pier shape coefficient may be assumed 1 for rectangular piers with round corners and 1/2 for those with sharp corners. Vaghefi et al. [17] have examined the flow pattern in a 180-degree sharp bend. The study concluded that after the beginning of the bend towards the end of it, the secondary flow power and the size of the created vortices increase. Ehteram and Mahdavi Meymand [18] demonstrated that the SSIIM model could predict streambed and scour depth variations. They found that the numerical scour depth was approximately 15% smaller than the experimental scour depth. Aksoy and Eski [19] investigated the scour depth and scour hole geometry around cylindrical bridge piers under clear-water conditions and different flow velocities. Proposing an experimental equation for scour depth

prediction, they concluded that the scour depth, downstream sedimentation length, and scour hole rose as the pier diameter and flow velocity increased. Maatooq and Mahmoud [20] studied local scouring around single central oblong bridge piers located at 180° bend using a laboratory model. The results showed that the maximum scour depth and the maximum extents of scour hole and maximum Modification factor occurs when pier located at sector 90° of the bend. Moussa [21] assessed the scour around the Aswan and El-Mina bridge piers located on the Nile River in Egypt. They utilized 1D and 2D mathematical models. Results indicated that the smallest local scour was obtained in case of sharp-nosed piers at normal flow to the piers. Kardan et al. [22] conducted the experimental and numerical estimation of local scour around sloped piers. They explored the effects of different parameters, including the slope degree, flow velocity, flow depth, and pier size, on local scour. It was revealed that a rise in the pier slope reduced the maximum scour depth. Yang et al. [23] conducted a comprehensive study of local scour around pier groups with different arrangements in steady-state flow conditions. The time development of scour was analysed by considering the effects of the pier distance and Froude number. It was demonstrated that the time development of the scour depth differed between the front pier and the back pier at small Froude numbers. This difference reduced as the Froude number increased. It was also indicated that the scour depth around the downstream pier was smaller than that around the upstream pier. One of the newest and fewest studies in the field of local scouring around bridge piers in the of convergence conditions of river meanders was conducted by Rasaei et al. [24]. They employed a laboratory flume with a 90° convergent meander to analyse scour at the angles of 0, 30, 45, 60, and 75 degrees. In general, the results revealed that with increasing convergence and subsequently increasing the angle of placement of the pier at the 90° convergent meander, the maximum depth and volume of scour increases. On the other hand, the results and output of the study showed that the maximum depth and volume of scouring occurs at an angle of 75 degrees. Also, Resaei et al. [25] adopted an SSIIM-2 model to simulate the scour pattern around piers in convergence conditions and compared the results to those of the experimental model. In summary, the results indicated that the SSIIM-2 model was sufficiently able to simulate the scour pattern around piers in convergence conditions. Although a large number of studies have been conducted on sedimentation and scour within straight and meandering channels, only a few studies have been conducted on scour around piers at convergent meanders. Thus, the present study aimed to investigate the effects of the pier shape and size on local scour around piers. An experimental model with a 90° convergent meander was employed. Cylindrical and cubic piers were fabricated and placed at the critical situation of the 90° convergent meander, evaluating local scour in clear-water conditions. Also, the tests were simulated using a numerical SSIIM model. Then, the experimental and numerical results were compared to validate the numerical model.

2. Materials and methods
2.1. Experimental Facilities and Procedure
2.1.1 Experimental flume

A Plexiglas channel with a 90° convergent meander and a centerline radius of 170 cm was employed [24, 25]. Straight channel sections with the lengths of 4.5 and 2 m were used upstream and downstream of the meander, respectively, to make the flow laminar. The width of the channel was 60 cm at the beginning of the meander and 30 cm at the end of the meander (i.e., a convergence ratio of ½). A sliding gate was embedded at the end of the channel to adjust the water level. Also, water was pumped by a 5-in centrifugal pump into the tank at the beginning of

the main channel and passed through the upstream straight channel section and meander into two successive tanks. A standard trapezoidal weir with a width of 20 cm was used at the end of the second tank to measure the flow rate, as shown in Figure 2.

Figure 2. Experimental flume with a 90° convergent meander [24, 25]

2.1.2. Sediments bed

In this research the sand with uniform grading and a mean grain diameter of 1 mm, standard deviation of 1.2, and a specific gravity of 2.65 with thickness of 15 cm was employed and covered total length of flume [24, 25].

2.1.3. Pier models

Since the aim was to investigate the effects of pier shapes and sizes on local scour, cylindrical piers with the diameters of 40 and 60 mm and cubic piers with the sizes of 40×40 and 60×60 mm were employed, according to the criteria proposed by previous studies [26-28]. Figure 3 shows examples of the piers used in this research.
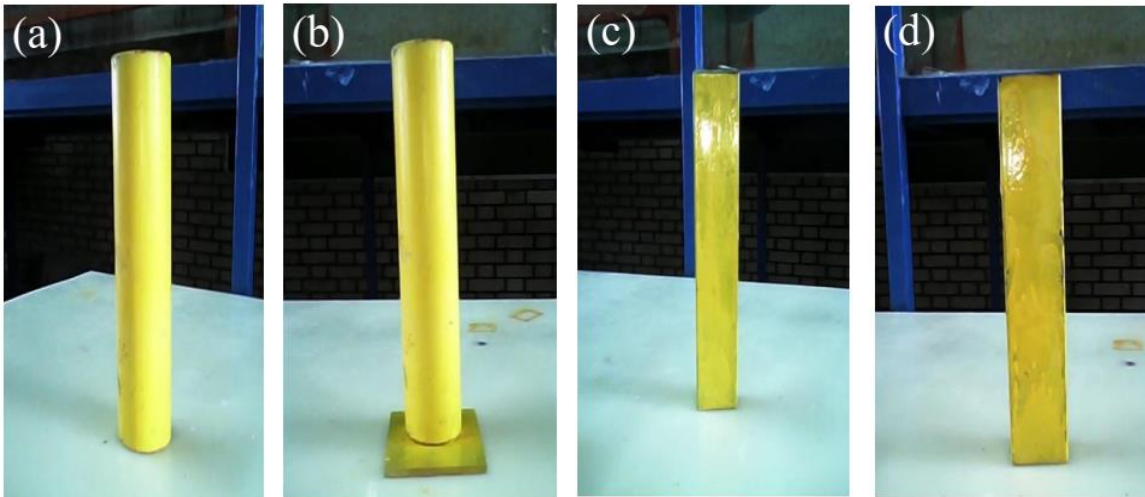
Figure 3. **Piers with different shape and dimensions. (a) Cylindrical pier with diameter of 40 mm, (b) Cylindrical pier with diameter of 60 mm, (c) Cubic pier with dimensions of 40×40 mm, (d) Cubic pier with dimensions of 60×60 mm**

2.1.4. Experimental procedure

To calibrate the model and provide clear-water conditions, a test was carried out without piers by using the sand with uniform grading, a mean grain size of D_{50}=1 mm, and a thickness of 15 cm [24, 25]. It was observed that the maximum flow rate required to prevent erosion and upstream sediment transfer and to provide clear-water conditions was 11.2 l/s for a fixed water depth of 10 cm along the channel – Olivito and Hager [29] suggested that the water depth should be higher than 20 mm to prevent roughness effects. Then, to calculate the equilibrium times of the tests, a longer test was performed on each of the two piers for 12 hours at a flow rate of 11.2 l/s and an angle of 75 degrees [24, 25]. It was observed that approximately 95% of scour occurred around the piers after 150 min. Thus, the equilibrium time was selected to be 150 min for the entire tests, as shown in Figure 4.
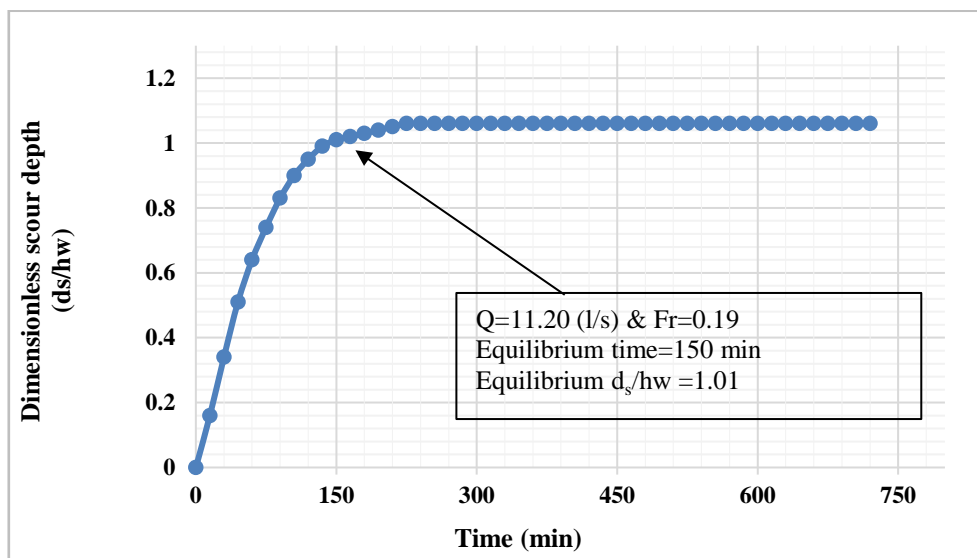
Figure 4.Equilibrium time in the position of 75° [24,25]

To perform the tests, the piers were placed at a critical angle of 75 degrees [24, 25]. Then, the bottom sediments were distributed uniformly along the channel. Before turning the pump on, the end gate was closed, and water was slowly directed into the channel to prevent ripples on the bed. Once the water level rose and sediments were ensured to have become wet, the pump was turned on at a small flow rate, and the flow rate was raised to the intended level by using the main valve on the inlet pipe. Then, the intended flow rate, clear-water conditions, and 10 cm flow depth were achieved by accurately and simultaneously adjusting the valve and downstream gate. The pump was turned off after 150 min (i.e., equilibrium time) to slowly drain the water from the channel. When the entire water was drained, the maximum scour depth around the pier and bed topography were measured using a laser meter with an accuracy of a few millimetres. The same procedure was performed on all the piers of different sizes. A total of twelve tests were performed on piers with different geometric and hydraulic conditions, as shown in Table 1.

Table 1. The effective geometric and hydraulic parameters on local scour

Effective parameters	Range of differences
Pier type and Dimensions	Cylindrical piers:(diameters of 40 and 60 mm) Cubic piers: (dimensions of 40×40 and 60×60 mm)
Pier material	Metal
Pier Position	75 (degree)
Channel slope	0.001 (m)
Discharge rate	6.10, 8.23 and 11.20 (l/s)
Froude number	0.1, 0.14 and 0.19
Average depth of flow	100 (mm)
Median grain size of bed	1 (mm)
Average thickness of bed particles	150 (mm)
Standard deviation of sediment particles	1.2 (dimensionless)
Density (mass per unit volume of fluid)	1 gr/ (cm^3)
Specific gravity of bed particles	2.65 gr/ (cm^3)

2.2. Numerical simulation procedure

2.2.1. Numerical model

The SSIIM software pack is a fluid dynamics program developed for hydraulic engineering problems. It was introduced by Olsen [5]. The unique characteristics of the SSIIM software pack include the use of advanced turbulence models and various solving algorithms in complex geometries. The discontinuing algorithm of SSIIM is the finite volume method, and the SIMPLE algorithm is employed to couple velocity-pressure equations. The standard method is used for pressure separation, while the control volume method and power-law (PL) algorithm or second-order upwind (SOU) algorithm are employed for the discretization of the momentum, pressure drop, turbulent kinetic energy, and Reynolds stress equations. SSIIM solves the Navier-Stokes equations on a three-dimensional non-orthogonal grid by using the k-ε turbulence model to obtain the water flow velocity. The Navier-Stokes equation for incompressible flows is represented as:

$$\frac{\partial U_i}{\partial t} + U_j \frac{\partial U_i}{\partial X_j} = \frac{1}{\rho} \frac{\partial}{\partial X_j} \left(-P\delta_{ij} - \rho \overline{U_i U_j} \right) \tag{1}$$

Where Ui is the average velocity component in the Xi direction; ρ is the density of water; P is the pressure; δ_{ij} is the Kroncker delta, which is 1 for i = j, and 0 otherwise; and Xi and Xj are the general space dimensions. The last term $\rho \overline{U_i U_j}$ in Eq. (1) is the Reynolds stress,
SSIIM has files with different structures. These files are mostly used for specific purposes. Some of these files are inputs, while the others are outputs. However, SSIIM has two essential files, including CONTROL and KOORDINA, which are required for the execution of SSIIM. KOORDINA is used to describe the geometry of points in the model, while CONTROL contains the required parameters of the model for calculations.

2.2.2. Meshing and three-dimensional model verification

The experimental channel was duplicated in the SSIIM model - i.e., a channel with a convergent meander angle of 90 degrees, a centerline radius of 170 cm. Since the channel had a convergent meander, it could not be modeled using structured grids in SSIIM. Thus, to draw the meander of the channel, its coordinates were extracted from Excel software and stored in the file KOORDINA according to the SSIIM instructions. For the straight downstream and upstream channel sections, structured grids (i.e., regular blocks) in the software were employed. Finally, the three blocks were assembled into an integrated model.
The next step was to estimate the best solution field grid based on the geometric model. Meshes of different sizes were examined by sensitivity analysis results. Table 2 and Figure 5 show the meshing analysis results of the meander, upstream, and downstream channels. The field geometry was defined in all the models such that the mesh size was smaller near the bridge piers and channel walls and inside the meander, particularly at higher angles. Larger meshes were applied to the other parts, such as the downstream and upstream straight sections. Moreover, smaller meshes were used in the flow direction and near the meander to reduce the computation time.
According to Table 2 and the sensitivity analysis results, among different meshing systems,

meshes in the sizes of 45×20×10 and 10×25×10 mm were employed for the downstream and upstream straight channel sections, respectively, in the longitudinal, transverse, and upward directions. Also, a mesh with a total of 28800 cells was used per angle for the meander and near the piers. A total of 88800 cells were employed as the optimal number of cells in the numerical analysis.

Table2 . Results of mesh sensitivity analysis

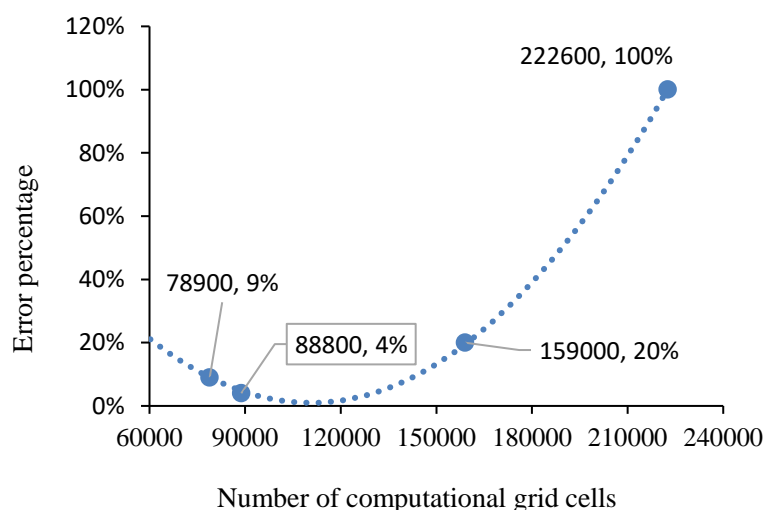| The number of cells considered in the convergent meander section	The number of cells considered in the direct channel upstream	The number of cells considered in the direct downstream channel	Total number of cells used in channel	Maximum scour depth in numerical work (cm)	Maximum scour depth in experimental work (cm)	Maximum scouring error (percentage)
27000	27000	24900	78900	7.13	7.85	9%
28800	30000	30000	88800	7.58	7.85	4%
15300	27000	15000	57300	5.94	7.85	24%
54000	67500	37500	159000	6.25	7.85	20%
57600	90000	75000	222600	Divergence	7.85	100%

Figure 5. Sensitivity analysis chart and number of optimal meshes

Figure 6 illustrates the final meshing grid used in the simulation with cylindrical and cubic piers. It should be noted that a reduction in the mesh size was observed to increase the execution time of the program but yielded more accurate results. Also, instability and divergence were observed when executing the program with small meshes.
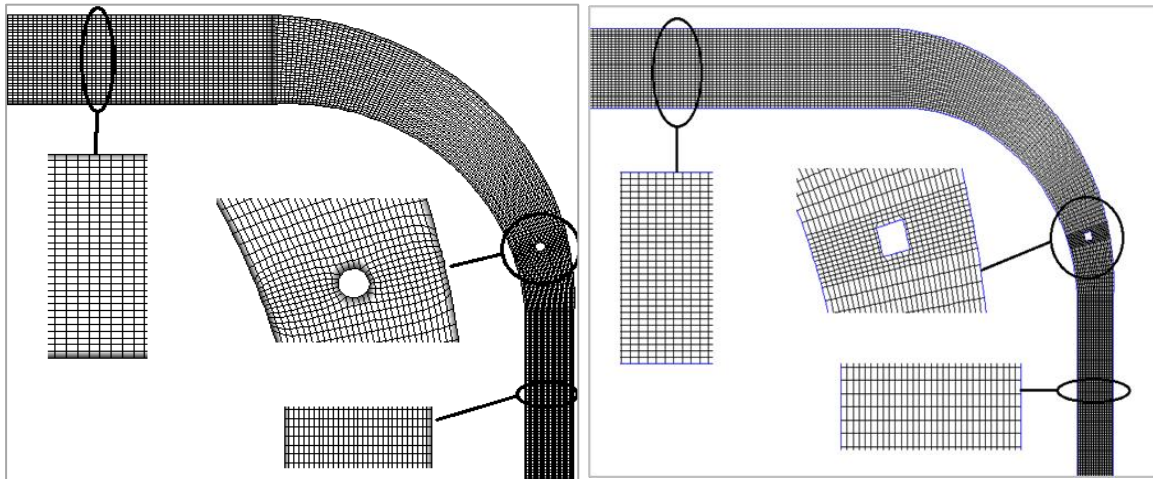
Figure 6. Schematic view of grids used in the numerical model, (a) Mesh grid with cylindrical pier, (b) Mesh grid with cubic pier

3. Results and discussion

In all the tests, after placing the pier at an angle of 75 degrees -the critical situation was obtained in Rasaei et al.'s research [25] and adjusting the flow rate and depth, scour began to occur at a large rate in the pier front. Then, as vortex flows developed, scour extended to every side and even behind the pier, as shown in Figure 7. Table 3 provides the maximum experimental and numerical scour depth results around the piers.
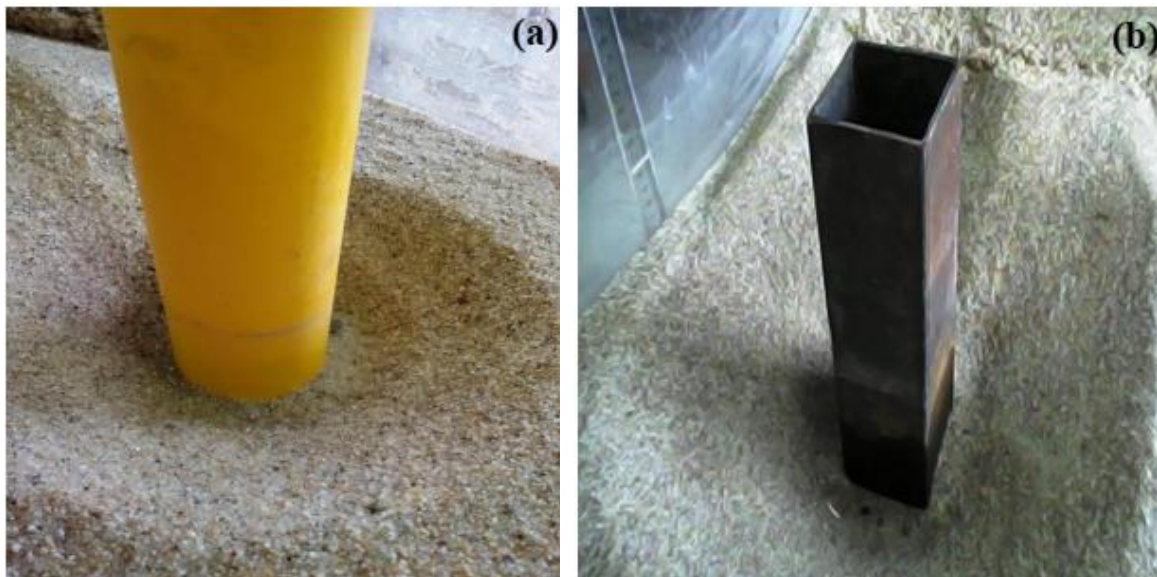

Figure 7. Scour hole around pier, (a) cylindrical pier, (b) cubic pier

Table3 . The results of maximum scour depth around piers in experimental and numerical models

Discharge rate Pier	Q=6.10 (l/s) & Fr=0.1		Q=8.23 (l/s) & Fr=0.14		Q=11.20 (l/s) & Fr=0.19	
	Experimental	Numerical	Experimental	Numerical	Experimental	Numerical
Cylindrical pier with diameter of 40 mm	2.2	2.1	4.3	4.15	6.25	6.2
Cylindrical pier with diameter of 60 mm	2.7	2.56	5.1	4.94	7.85	7.57
Cubic pier with dimensions of 40×40 mm	2.5	2.3	4.8	4.7	7.25	6.4
Cubic pier with dimensions of 60×60 mm	3.3	3.24	6.3	6.24	9.15	9.00

3.1. Flow field around the pier located in convergent meander

The investigation of longitudinal and transverse flow patterns on the rigid bed of the convergent meandering channel and around the bridge piers can considerably help obtain a qualitative insight into the erosion and sedimentation patterns of such meanders and the size and procedure of scouring around the piers. Figure 8 depicts the longitudinal flow pattern within the convergent meander and around the cylindrical piers with the diameters of 40 and 60 mm and the cubic piers with the sizes of 40×40 and 60×60 mm. It should be noted that X1 and X2 represent the coordinates of the channel in the longitudinal and transverse directions, respectively. As can be seen, in the meander and pier upstream, parallel streamlines uniformly flow downstream. However, near the pier, the streamlines changed their direction to the transverse direction and became dispersed around the pier. Given that the flow velocity is higher at free surfaces, flow separation was larger downstream of the pier. At the same time as flow separation, a flow moving downward formed, which triggered erosion and scour upstream of the pier. As the flow rate and thus convergence increased, the streamlines became continuous and larger around the pier, surrounding the pier. A comparison of the longitudinal streamlines around the cylindrical and cubic piers suggests that the streamlines moved through more regular paths after meeting the cylindrical pier, compared to those meeting the cubic pier. Due to the aerodynamic effect of the cylindrical pier, these streamlines formed around the cylindrical pier regularly with a radius proportional to the pier radius and then separated from downstream of the pier in the same regular paths, leaving the channel, as shown in Figures 8(a) and 8(b). Figures 8(c) and 8(d) represent longitudinal streamlines around the cubic piers with the sizes of 40×40 and 60×60 mm. It was observed that the longitudinal streamlines around the cubic piers were more complex than those around the cylindrical piers. Once the flow met the cubic pier, various

vortexes formed around the pier since the pier and its sides were not aerodynamic. It was observed that larger flow separation occurred after the flow met the cubic pier, compared to the cylindrical pier. This could play a significant role in the extension of the scour hole around the pier. Overall, it can be said that a rise in the diameter and size of the pier increases the dispersion of the streamlines after they meet piers, leading to larger scour holes around the piers.
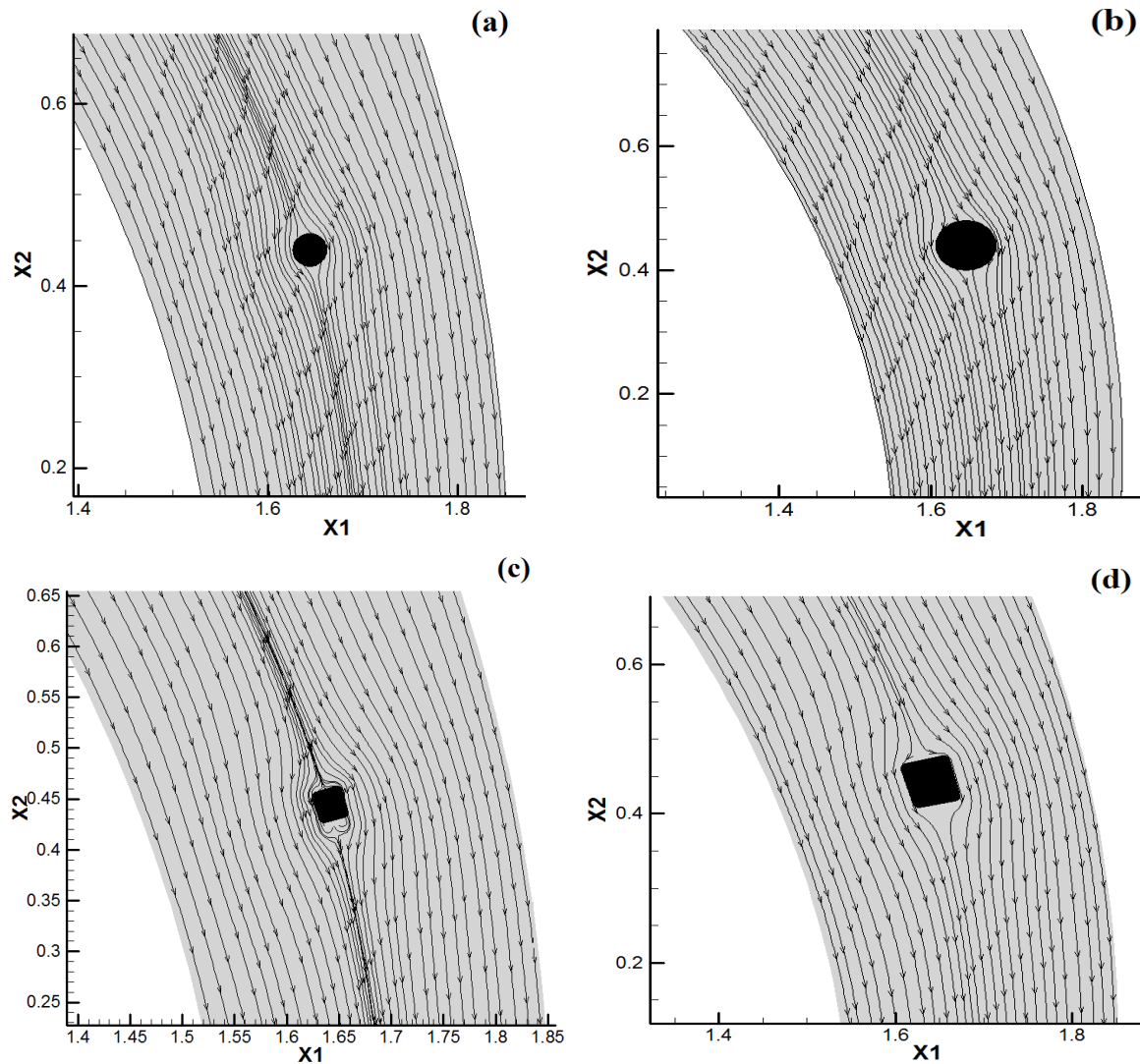
Figure 8. Longitudinal streamlines around different pier, (a) Cylindrical pier with diameter of 40 mm, (b) Cylindrical pier with diameter of 60 mm, (c) Cubic pier with dimensions of 40×40 mm, (d) Cubic pier with dimensions of 60×60 mm

The analysis of the transverse flow velocity distribution within convergent meanders and around piers is another method for distinguishing and evaluating the flow pattern and scour around piers at convergent meanders, as shown in Figure 9. The evaluation of transverse velocity variations indicates that the transverse flow moved through the first half of the meander toward the inner curve at a regular rate. In the second half of the meander, the transverse flow enlarged.

The convergence and contraction enhancement of the channel affected the magnitude of the transverse flow, and the transverse flow magnitude was maximized at the end of the meander. According to Figure 9, the transverse flow magnitude around the pier significantly increased when it arrived in the pier area in the meander and met the pier. The secondary helical flow induced by the transverse flow is the main cause of erosion and scour around piers within a meander. Then, as it passed the pier, the transverse flow left the channel from its end in an extended form. As can be seen in Figure 9, the transverse flow was larger and more extended around the cubic pier than around the cylindrical pier with the same diameter. This can significantly contribute to the development of scour around cubic piers, compared to scour around cylindrical piers.
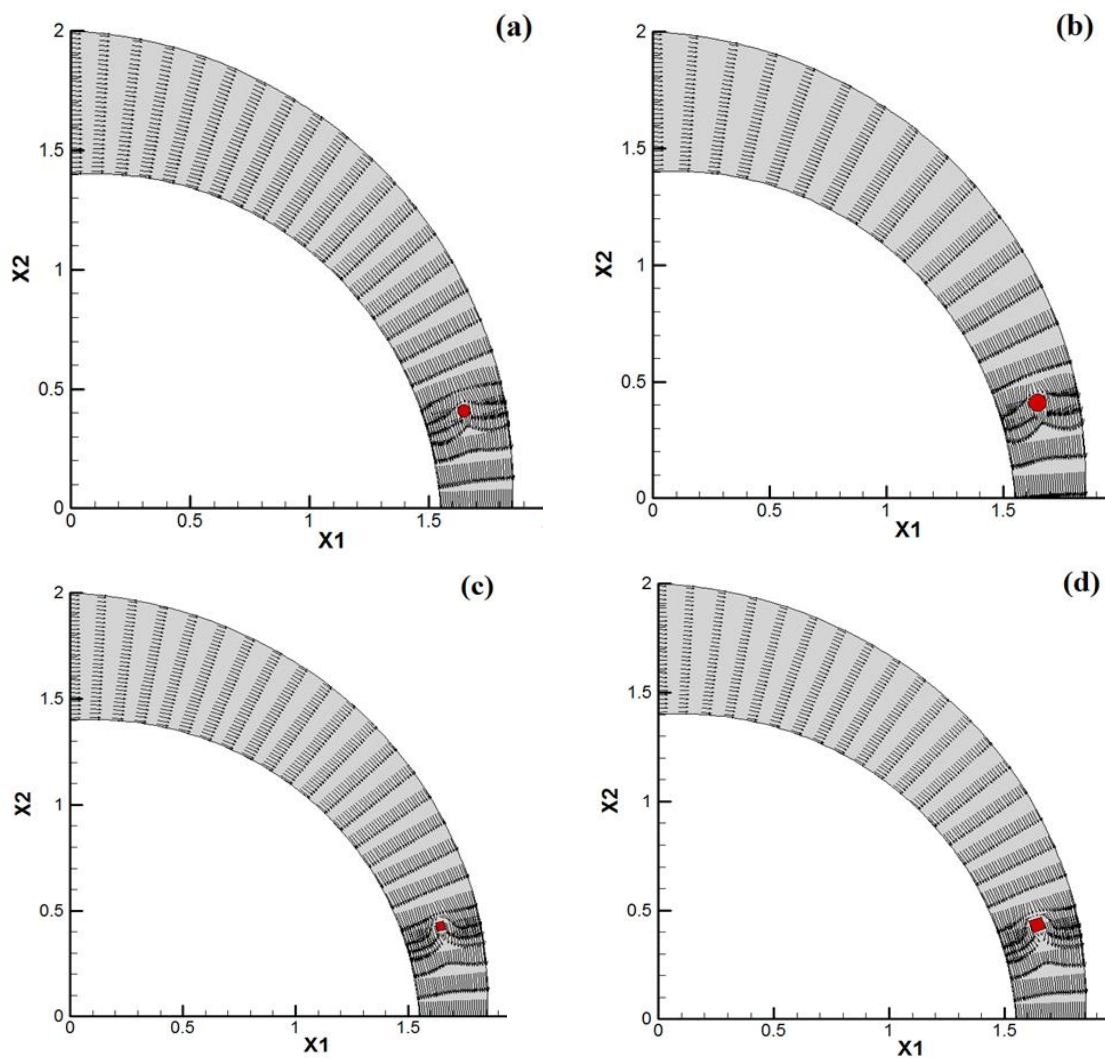
Figure 9. Transvers streamlines around different pier, (a) Cylindrical pier with diameter of 40 mm, (b) Cylindrical pier with diameter of 60 mm, (c) Cubic pier with dimensions of 40×40 mm, (d) Cubic pier with dimensions of 60×60 mm

3.2. Local scouring around piers in different geometric shapes

The experimental and numerical results revealed that the geometry and size of a pier has a large effect on scour. Figures 10 [24] and 11 illustrate the geometry contours of the scour holes around the cylindrical piers with the diameters of 40 and 60 mm and cubic piers with the sizes of 40×40 and 60×60 mm at a Froude number of 0.19. Overall, a rise in the pier size reduced the cross-section of the pier and increased the flow velocity. As a result, a flow with higher turbulence formed around the pier, which produced a stronger downward flow in front of the pier that impacted the streambed as a water jet, separating sediments and enhancing the scour hole over time. It was observed that horseshoe vortexes followed regular paths around the pier when meeting the cylindrical pier since it was aerodynamic. The scour hole around the cylindrical pier had a more regular geometry than the one around the cubic pier. Also, the size and depth of the scour hole around the cylindrical pier were estimated to be smaller than those of the scour hole around the cubic pier, as shown in Figures 10 and 11. Furthermore, due to their non-aerodynamic geometry, cubic piers obstruct flows. When a flow meets a cubic pier, strong shear stresses and horseshoe vortexes form at a larger distance from the pier, and an asymmetric scour hole often appears, which sometimes extends to the channel walls, as shown in Figure 11. Overall, it can be said that when the pier size rises, the effect of the boundary layer on flow separation, on the one hand, and the enlarged vortex flows, on the other hand, enlarge the scour hole around the pier in the longitudinal and transverse directions; however, the scour hole size differs between piers in different shapes. Furthermore, as demonstrated by Rasaei et al. [24, 25], a comparison of scour in different conditions indicated that meander convergence affects local scour around piers and increases the continuity of streamlines and thus scour around bridge piers.

According to Figures 10 and 11, the scour hole was larger around the cubic piers than around the cylindrical piers. The calculations revealed that the scour hole around the cubic pier with a size of 40×40 mm was approximately 15% larger than that around the cylindrical pier with a diameter of 40 mm. Also, the scour hole around the cubic pier with a size of 60×60 mm was observed to be larger than the cylindrical pier with a diameter of 60 mm by up to 29%. A comparison of the experimental and numerical results suggests that the numerical SSIIM model can simulate the scour pattern around piers at 90° convergent meanders.
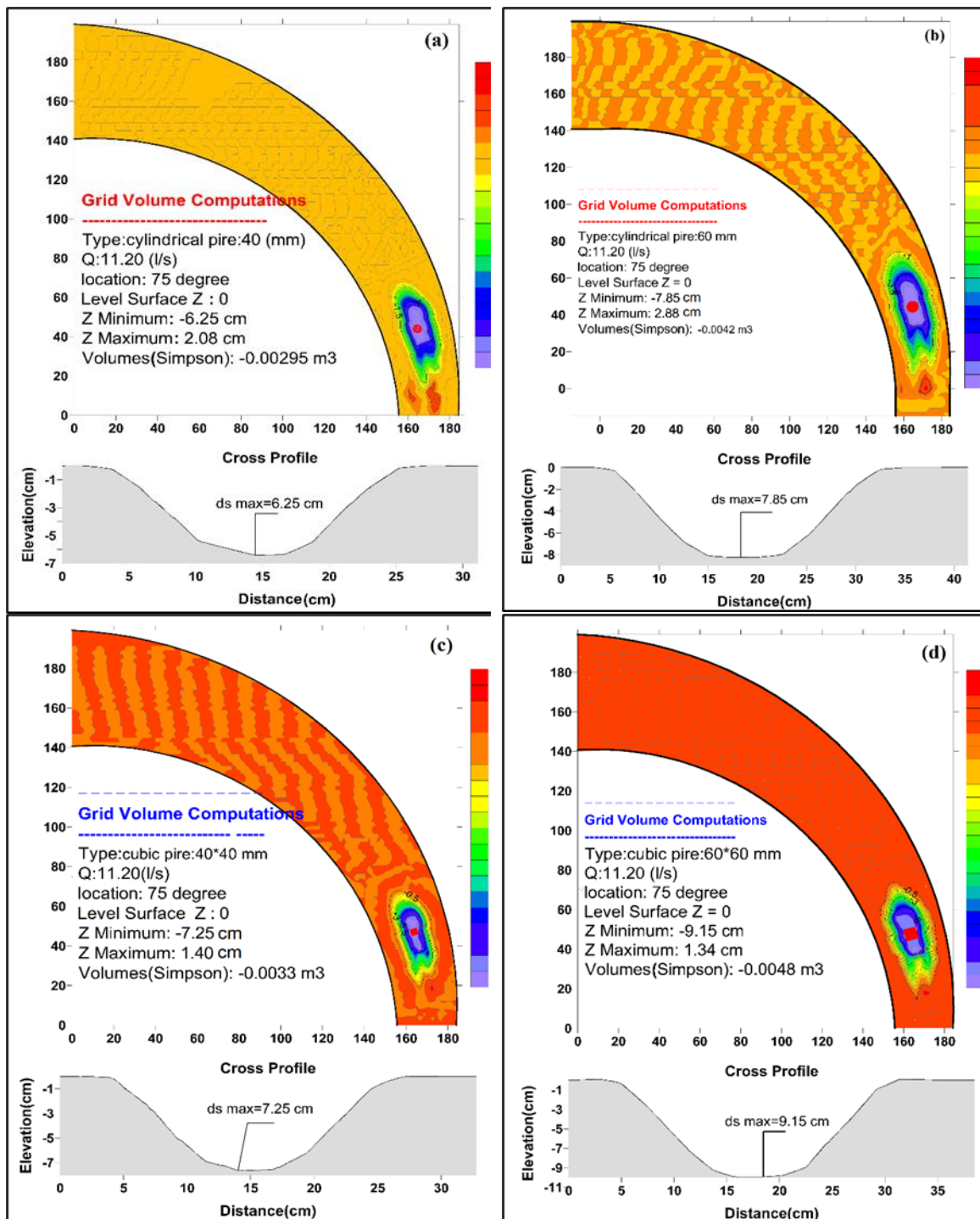
Figure 10. Scour hole around different piers under discharge rate of 11.20 l/s in experimental work. (a) Cylindrical pier whit diameter of 40 mm, (b) cylindrical pier with diameter of 60 mm, (c) Cubic pier with dimensions of 40×40 mm, (d) Cubic pier with dimensions of 60×60 mm [24]
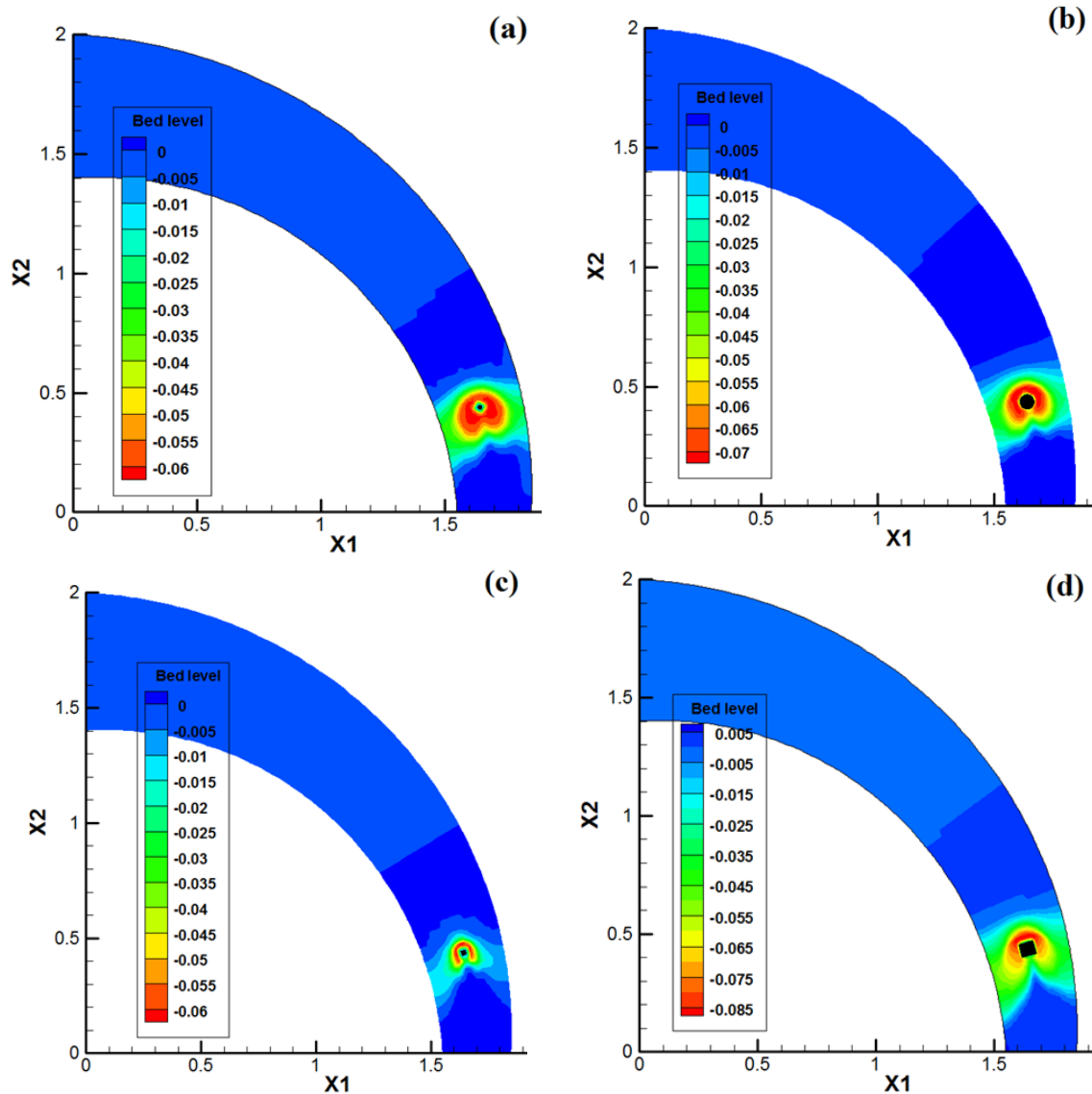
Figure 11. Scour hole around different piers under discharge rate of 11.20 l/s in numerical model. (a) Cylindrical pier whit diameter of 40 mm, (b) cylindrical pier with diameter of 60 mm, (c) Cubic pier with dimensions of 40×40 mm, (d) Cubic pier with dimensions of 60×60 mm

Figure 12 compares the numerical and experimental maximum scour depths around the cylindrical and cubic piers with different diameters and sizes. According to Table 2 and Figure 12, a rise in the diameter or size of the pier increased the scour depth. The experimental results indicate that a 50% rise in the diameter of the cylindrical pier raised the maximum scour depth by 23%, 19%, and 26% at the Froude numbers of 0.1, 0.14, and 0.19, respectively. Also, the same rise in the diameter of the numerical cylindrical pier raised the maximum scour depth by 22%, 19%, and 22% at the Froude numbers of 0.1, 0.14, and 0.19, respectively. On the other hand, a 50% rise in the size of the cubic pier raised the maximum scour depth by 32%, 31%, and 26% in the experimental model and by 41%, 33%, and 41% in the numerical model at the

Froude numbers of 0.1, 0.14, and 0.19, respectively. A comparison of the experimental and numerical maximum scour depth results indicates that the two models yielded close results, and the numerical SSIIM model is capable of simulating the scour pattern around a bridge pier.

It was observed that the maximum scour depth was smaller around the cylindrical piers than around the cubic piers. The maximum local scour depth around the cylindrical pier with a diameter of 40 mm was smaller than that around the cubic pier with a size of 40×40 mm by up to 29%, 41%, and 2% at the Froude numbers of 0.1, 0.14, and 0.19, respectively, indicating an average reduction of 24%. Furthermore, the maximum local scour depth around the cylindrical pier with a diameter of 60 mm was smaller than that around the cubic pier with a size of 60×60 mm by 46%, 42%, and 46% at the Froude numbers of 0.1, 0.14, and 0.19, respectively, showing an average decrease of 44%. It should be noted that the maximum scour depth around the piers occurred in the front and upstream of the cylindrical pier and the upstream and corners of the cubic piers.
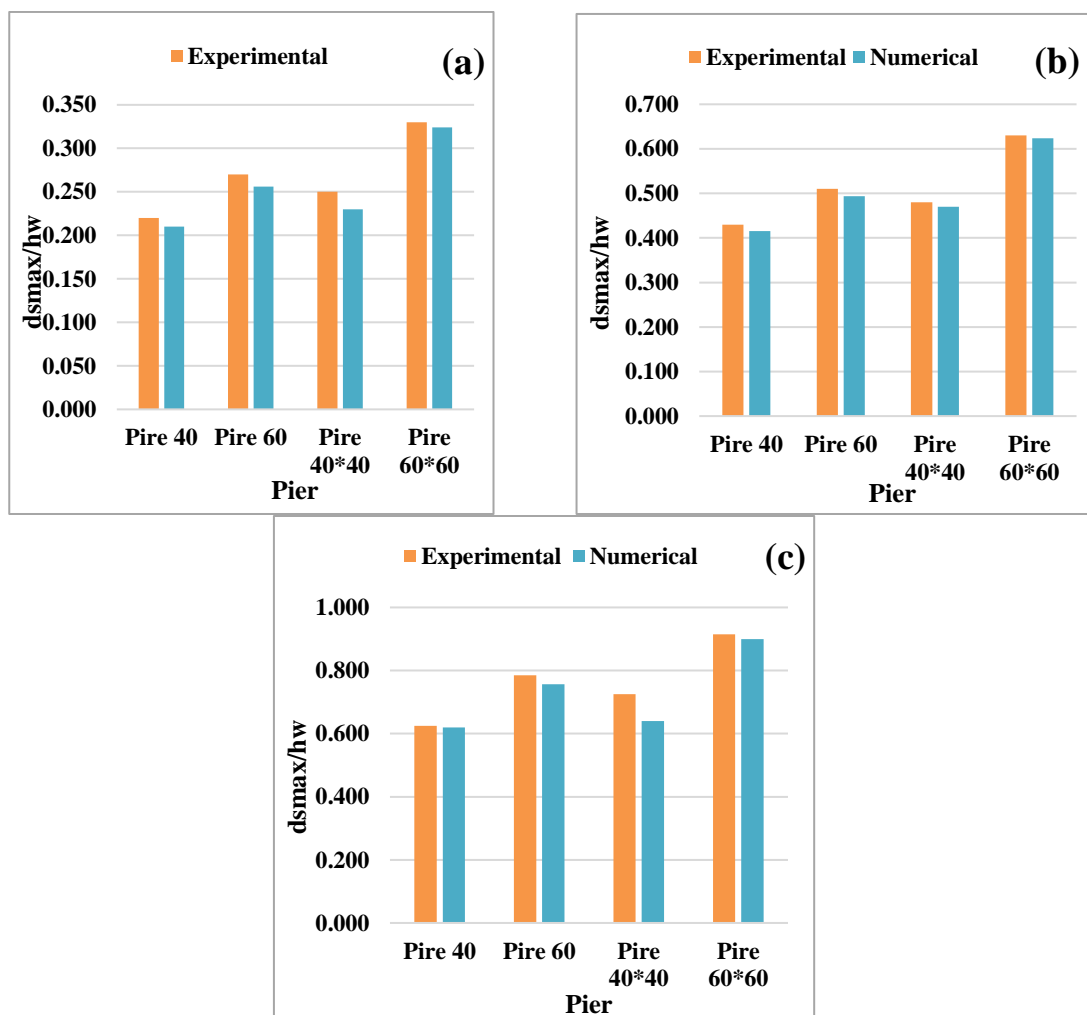

Figure 12. Changes of the maximum scour depth relative to different piers in both laboratory and numerical models. (a) Fr=0.1, (b) Fr=0.14, (c) Fr=0.19

The flow rate, or the Froude number, is a factor that has a strong effect on the maximum scour depth in convergent channels. The experimental and numerical results supported this claim and indicated that a rise in the flow rate raised the flow velocity, and consequently, horseshoe vortexes and uplift around the piers. Moreover, a reduction in the meander width along the channel (i.e., convergence enhancement) reduced the flow cross-section and significantly raised the velocity at which the flow met the piers, enhancing the scour depth around the piers. Overall, it can be said that a rise in the Froude number, and consequently, in the flow velocity increased the stress concentration at the cross-section contraction (i.e., pier location). As a result, local scour-induced topographic changes in the streambed and around the pier enlarged.

Figure 13 plots the experimental and numerical maximum scour depths around the cylindrical piers with the diameters of 40 and 60 mm and cubic piers with the sizes of 40×40 and 60×60 mm versus the Froude number. As can be seen, a rise in the Froude number significantly raised the experimental and numerical scour depths around the piers, with acceptable differences between the two models. It was observed that a 90% rise in the Froude number increased the maximum scour depth around the cylindrical pier with a diameter of 40 mm by 184% and 195% in the experimental and numerical models, respectively. Also, a 90% rise in the Froude number increased the maximum scour depth around the cylindrical pier with a diameter of 60 mm by 191% and 196% in the experimental and numerical models, respectively. The same rise in Froude number was estimated to increase the experimental and numerical maximum scour depths by 190% and 178% around the cubic pier with a size of 40×40 mm and by 191% and 196% around the cubic pier with a size of 60×60 mm, respectively. Overall, the experimental and numerical maximum scour depth results were found to be close.
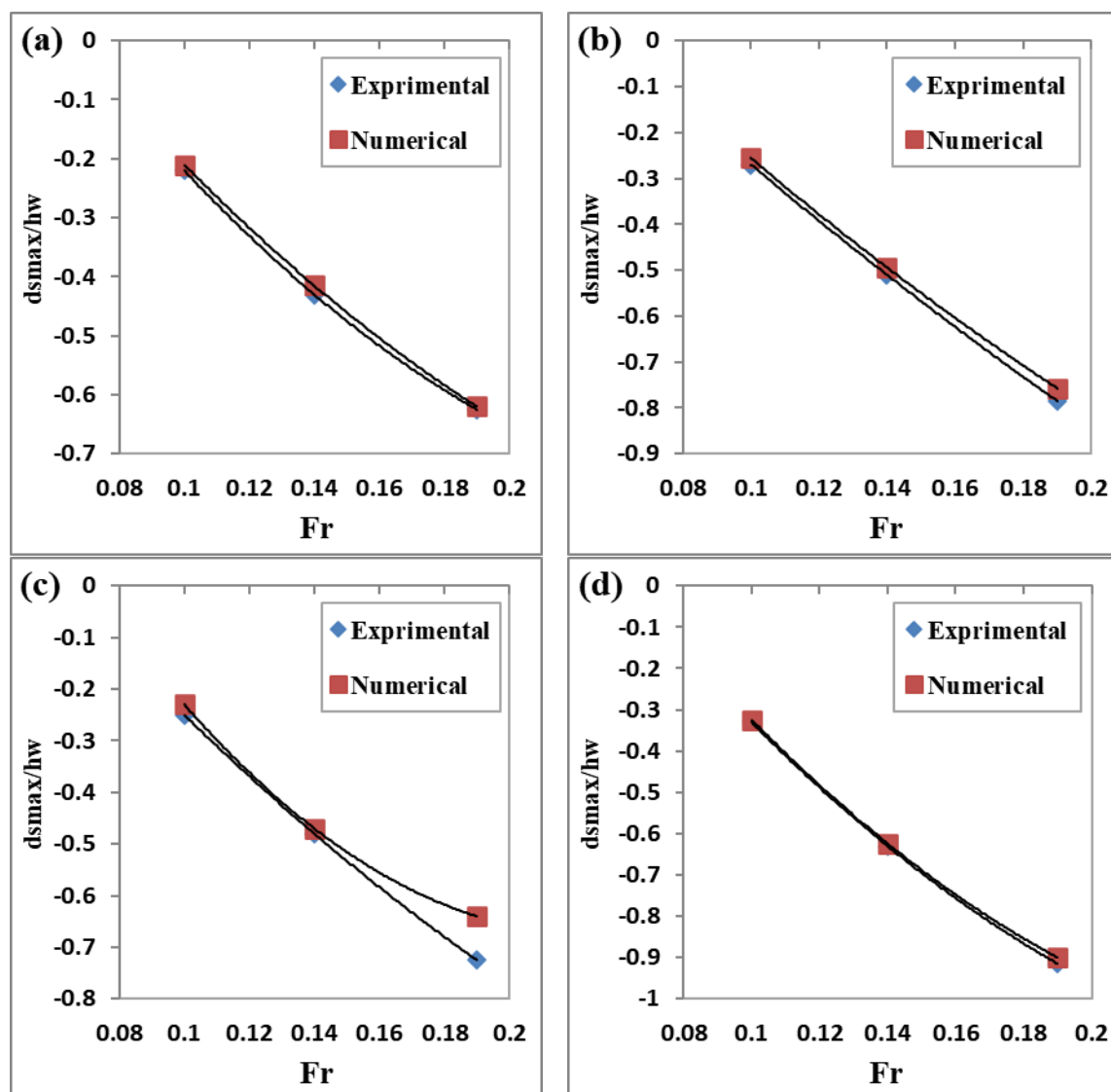
Figure 13. Comparison of maximum scour depth under different Froude numbers in experimental and numerical models. (a) Cylindrical pier whit diameter of 40 mm, (b) cylindrical pier with diameter of 60 mm, (c) Cubic pier with dimensions of 40×40 mm, (d) Cubic pier with dimensions of 60×60 mm

4. Conclusion

The placement of bridge piers at 90° convergent meanders has been among the most important topics in hydraulics. The present study experimentally and numerically investigated the effects of the geometries and sizes of piers on local scour at a 90° convergent meander. The results can be summarized as

- A rise in the pier size increased the maximum scour depth.
- Local scour was smaller around the cylindrical piers than around the cubic piers.

- The diameter or size of a pier has a significant effect on the formation of secondary and vortex flows around the pier; a rise in the pier size significantly raises the magnitude and extension of vortex flows.
- The formation of longitudinal and transverse streamlines, and consequently, horseshoe vortexes around a pier is affected by the shape of the pier; streamlines around a cylindrical pier are more regular and smaller than those around a cubic pier since cylindrical piers are aerodynamic.
- The convergence and contraction of a channel reduce the cross-section and increases the velocity at which the flow meets the pier, increasing the maximum scour depth.
- A rise in the Froude number raises the maximum scour depth.
- The numerical SSIIM model was able to simulate local scour around bridge piers.

Nomenclature

d_s	Maximum scour depth (cm)
L	Length of pier (mm)
b	width or diameter of pier (mm)
B	Width of channel (cm)
V	Velocity of flow (m/s)
θ	Location of pier in meander (degree)
g	Gravitational acceleration (m/s^2)
d_{50}	Median grain size (mm)
h_w	Flow depth (cm)
t	Time at maximum scouring (min)
ρ	Density of water (gr/cm^3)
ρ_s	Density of sediment (gr/cm^3)
Fr	Froude number
σ_g	standard deviation of sediment particles
Q	Flow discharge rate (l/s)
p	Pressure (kpa)
U_i	the average velocity component (m/s^2)
X_i	Direction (m)

References

1. Meander river, Volga River. https://fa.wikipedia.org/ (accessed 7 August 2020).
2. Tison L J, (1961). Local scour in rivers. Journal of Geophysical Research, 66(12): 4227–4232.
3. Yen, C. l., Bed configuration and characteristics of sub critical flow in a meandering channel. PhD. thesis, University of Iowa, 1967.
4. Georgiadou A D, Smith K V H, (1986). Flow in curved converging channel. Journal of Hydraulic Engineering, 112(6): 476-496.

5. Melville B W, Chiew Y M, (1999). Time scale for local scour at bridge piers. Journal of Hydraulic Engineering-ASCE, 125: 59-65.

6. Olsen, N.R.B., A three–dimensional numerical model for simulation of sediment movements in water intakes with multiblock option, Department of Hydraulic and Environmental Engineering, the Norwegian University of Science and Technology, 2006.

7. Abouzeid, A. A., Mohamed Hassan, I., Ali Shima, M. (2006). 3-D numerical simulation of flow and clear water scour by interaction between bridges piers. Proceeding of 10th international water technology conference, Alexandria, Egypt.

8. Dey S, Raikar R V, (2007). Characteristics of horseshoe vortex in developing scour holes at piers. Journal of hydraulic engineering, ASCE, 133(4): 399-430.

9. Sanoussi, A, A., Habib E A, (2008). Local scour at rounded and sloped face with skew angles. International Conference Construction and Building Technology, Kuala Lumpur, Malaysia.

10. Sanei, M. (2008). Laboratory analysis of the effects of critical velocity and grading on the degree of scouring. Proceeding of 14th National Congress on Civil Engineering, University of Tehran. Tehran, iran.

11. Fazli M, Ghodsian M, Neyshabouri S A A S, (2008). Scour and flow field around a spur dike in a 90° bend. International Journal of Sediment Research, 23: 56-68.

12. Masjedi A, Bejestan M S, Kazemi H, (2010). Effect of Bridge Pier Position in a 180 Degree Flume Bend on Scour Hole Depth. Journal of Applied Sciences, 10(8): 670-675.

13. Ghobadian R, Mohammadi K, Hossinzade D A, (2010). Numerical simulation and comparison of flow characteristics in 180º divergent and uniform open-channel bends using experimental data. Journal of Irrigation Science and Engineering, 33(1), 59-75.

14. Sabita M S, Maiti P R, (20120. local scouring around a circular pier in open channel. International Journal of Emerging Technology and Advanced Engineering, 2(5): 454-458.

15. Zulhilmi I, Mazlin J, FaridahJaafar S, Ahmad khairiAbd W, Zulkiflee I, (2013).Scour Investigation around Single and Two Piers Side by Side Arrangement. International Journal of Research in Engineering and Technology, 2(10): 459-465.

16. Fael, C., Lanca, R., Cardoso, A. (2014). Pier shape and alignment effects on local scour. Proceedings small scale morphological evolution of coastal, estuarine and rivers systems conference, Nantes, France.

17. Vaghefi M, Akbari M, Fiouz A R, (2014). Experimental Investigation on Bed Shear Stress Distribution in a 180 Degree Sharp Bend by using Depth Averaged Method. International Journal of Scientific Engineering and Technology, 3(7): 962-966.

18. SHF Conference: «Small scale morphological evolution

19. Of costal, estuarine and river systems_Nantes 6 & 7 october 2014 – Fael, Lança, Cardoso – Pier Shape and Alignment effects on Local Scour

20. SHF Conference: «Small scale morphological evolution

21. Of costal, estuarine and river systems_Nantes 6 & 7 october 2014 – Fael, Lança, Cardoso – Pier Shape and Alignment effects on Local Scour

22. Ehteram M, Mahdavi Meymand A, (2015). Numerical modeling of scour depth at side piers of the bridge. Journal of Computational and Applied Mathematics, 280: 68–79.

23. Aksoy A O, Eski O Y, (2016). Experimental investigation of local scour around circular bridge piers under steady state flow conditions. Journal of the South African Institution of Civil Engineering, 58(3): 21–27.

24. Maatooq J S, Mahmoud E S, (2017). Local Scour around Single Central Oblong Bridge Piers Located within 180° Bend. International Journal of Hydraulic Engineering, 6(1): 16-23.

25. Moussa M A M, (2018). Evaluation of local scour around bridge piers for various geometrical shapes using mathematical models. Ain Shams Engineering Journal, 9(4): 2571-2580.

26. Kardan N, Rezaie M, Dini M, (2019). Experimental study of the local scouring around sloped piers and its estimation using statistical tools. Sādhanā, 44(1), 214.

27. Yang Y, Qi M, Wang X, Li J, (2020). Experimental study of scour around pile groups in steady flows. Ocean Engineering, 195(1): 1-12.

28. Rasaei M, Nazari S, Eslamian S, (2020). Experimental investigation of local scouring around the bridge piers located at a 90° convergent river bend. Sadhana, 45(1), 87.

29. Rasaei.M, Nazari S, Eslamian S, (2020). Experimental and numerical investigation the effect of pier position on local scouring around bridge pier at a 90° convergent bend. Journal of hydraulic structures, 6(1): 55-76.

30. Raudkivi A J, Ettema R, (1983). Clear-water scour at cylindrical piers. Journal of Hydraulic Engineering.-ASCE, 109: 339-350.

31. Melville B W, Sutherland A J, (1988). Design method for local scour at bridge piers. Journal of the Hydraulics Division, 114: 1210-1225.

32. Guemou B, Seddini A, Ghenim N A, (2016). Numerical investigations of the round-nosed bridge pier length effects on the bed shear stress. Progress in Computational Fluid Dynamics, 16: 313-321.

33. Oliveto G, Hager W H, (2002). Temporal Evolution of Clear-Water Pier and Abutment Scour. Journal of Hydraulic Engineering-ASCE, 128: 811-820.